Classification of Tropical Vegetation Using Multifrequency Partial SAR Polarimetry

Cédric Lardeux, Pierre-Louis Frison, Céline Tison, Jean-Claude Souyris,
Benoît Stoll, Bénédicte Fruneau, and Jean-Paul Rudant

Abstract—This letter presents a case study addressing the comparison between different synthetic aperture radar (SAR) partial polarimetric options for tropical-vegetation cartography. These options include compact polarization (CP), dual polarization (DP), and alternating polarization (AP). They are all derived from fully polarimetric (FP) SAR data acquired by the airborne SAR (AIRSAR) sensor over the French Polynesian Tubuai Island. The classification approach is based on the support vector machine algorithm and is further validated by several ground surveys. For a single frequency band, FP data give significantly better results than any other partial polarimetric configuration. Among the partial polarimetric architectures, the CP mode performs best. In addition, the DP mode shows better performance than the AP mode, highlighting the value of the polarimetric differential phase. The combination of different frequency bands (P-, L-, and C-bands) holds the most significant improvement: The multifrequency diversity adds generally more information than the multipolarization diversity. A noticeable result is the major contribution of the C-band at VV polarization (the only polarization available at C-band with the AIRSAR data set used in this letter) to the classification performance, due to its ability to discriminate between Pinus and Falcata.

Index Terms—Compact polarization (CP), partial polarimetry, radar polarimetry, supervised classification, support vector machine (SVM), synthetic aperture radar (SAR), tropical vegetation, Tubuai.

I. INTRODUCTION

FULLY polarimetric (FP) radar data are of prime interest for land-use classification [1]–[3]. These data have been widely used with the availability, since 2007, of a new generation of spaceborne FP radar sensors such as the Advanced Land Observing Satellite (ALOS) Phased Array type L-band synthetic aperture radar (SAR) (PALSAR), Radarsat-2, or TerraSAR-X, operating at L-, C-, and X-bands, respectively.

Nevertheless, FP modes have heavy constraints, compared with single polarized sensor, due to the alternating emission of two orthogonal polarizations and the halving of the swath (i.e., doubling the revisiting time). Consequently, partial polarimetry can be considered to reduce complexity. For example, a partial polarimetric mode, generally referred to as dual polarization (DP), consists of transmitting one single polarization, while the reception is conducted on two orthogonal polarizations (i.e., the co- and cross-polarization of the transmission). A recurring issue is to assess the potential of such reduced architecture in comparison with FP data [4]–[7].

In a previous study, FP Airborne SAR (AIRSAR) data were used for the classification of tropical vegetation over a French Polynesian Island [8]. Several ground surveys allowed for the constitution of a consistent validation data set. Results showed the efficiency of FP radar data at L- and/or P-band. They also showed that the combination of different frequency bands holds significant improvement. Moreover, the use of the support vector machine (SVM) classification method [9] was found to be much more efficient than alternative standard algorithms requiring an *a priori* assumption on the polarimetric coherency matrix distribution (e.g., Wishart distributed).

Extending this previous work, we assess here, over the same study site, several partial polarimetric modes for tropical-vegetation classification: alternate polarization (AP) and DP, available on Advanced SAR (ASAR)/Environmental Satellite (ENVISAT) and PALSAR/ALOS, Terrasar-X, or Radarsat-2, and compact polarization (CP) modes, [5], [10]. All these modes were generated from FP data.

The study site and the concurrent ground truth are presented in Section II. The method used to compare the different polarimetric options is developed in Section III. Results are discussed in Section IV. Section V concludes.

II. STUDY SITE AND DATA

A. Study Site

Tubuai Island is part of the *Australe* islands and is located at 23.38° S and 149.45° W, in the south of French Polynesia. It presents a large diversity of land-use classes and vegetation types and is widely documented through regular *in situ* surveys. Land-use classes are listed in Table I. Vegetation occupies 94% of the island with an equal share of forest and low vegetation. The forests spread over three main species: "Purau," "Pinus," and "Falcata," with a few "Strawberry Guava" specie patches (< 1%). Fig. 1 shows an illustration of the different structures of Purau, Pinus, and Falcata species, the latter two being rather

TABLE I
LAND USE OF THE TUBUAI ISLAND

Class type	Class number - name	Percent cover	# training samples	# control samples
Forest	1 - Pinus	13 %	3 000	5 000
	2 - Falcata	7 %	2 000	2 000
	3 - Purau	26 %	3 000	5 000
	4 - Guava	< 1 %	500	500
Low vegetation	5 - Fern lands	42%	2 000	2 500
	6 - Swampy vegetation	5%	2 000	5 000
Bare soils, roads	7 - Bare soils	5 %	2 000	5 000

close to erectophile and planophile distributions, respectively. Low vegetation mainly consists of fern lands and swampy vegetation. Several ground surveys have been carried out, and their combination with a Quickbird image allows the constitution of a valuable validation data set. It can be noted that on February 5, 2010, a particularly intense storm hit the island and drastically changed the landscape.

B. AIRSAR Data

The Jet Propulsion Laboratory AIRSAR data were acquired in August 2000 at P-, L-, and C-band frequencies (430 MHz, 1.24 GHz, and 5.29 GHz, respectively). FP data are available at P- and L-band frequencies, while C-band data were only acquired in VV polarization. The FP calibrated products are delivered as multilook complex format. The slant-range resolution is 5.5 m for the three bands, and the azimuth resolution is 10.8, 13.5, and 31.5 m, respectively, for C-, L-, and P-band. For the three bands, the delivered data correspond to 9×1 look in the azimuth and ground-range directions, respectively, with a pixel size of 5×5 m^2. The incidence angle ranges between $26°$ and $62°$. Fig. 2 shows an AIRSAR composite RGB image of the Tubuai Island.

III. METHOD FOR PARTIAL-MODE COMPARISON

The methods (i.e., SVM algorithm and polarimetric indicators selection) were presented in [8] and proved to be very efficient. They are summarized next. This letter focuses on the comparison of polarization mode and not on classification method.

A. SVM Method

Among other advantages, the SVM algorithm allows defining feature vectors with heterogeneous components (i.e., with different physical dimension), also called primitives, such as the polarimetric indicators considered for this study. For a two-class problem, the SVM method is based on the determination of the optimal hyperplane of the input data space that will maximize the distance separating the two training classes. When such a hyperplane cannot be found, training vectors are projected into a space of higher dimension (the feature space) in which the search for the optimal hyperplane will be replayed. The projection of the problem in the feature space is significantly simplified by the use of a kernel function (see [8]

and [9] for details). The generalization of the SVM algorithm to an N-class problem ($N \geq 2$) is straightforward [11].

B. Polarimetric Indicators and Partial Polarimetric Modes

When a single FP band is concerned, 54 polarimetric indicators were considered [8], leading to the definition of a 54 component feature vector $V_{\rm FP}$. These include the three channel intensities and their ratio, the variation coefficient c_v (ratio between standard deviation and the average of the intensity), and the degree of coherence ρ (amplitude and phase) for linear and circular polarizations. Other polarimetric indicators were added, including the span S, the three parameters $H/A/\alpha$ of the Cloude and Pottier decomposition [3], and the five Euler parameters m, γ, ν, ψ, and τ [13]. The selection of 25 among these 54 polarimetric indicators allowed obtaining the best classification results [8].

The different partial polarimetric modes are derived from the FP AIRSAR data at L- and P-bands, leading to the simulation of AP and DP similar to the configurations available on ASAR and PALSAR, Radarsat-2, or Terrasar-X. The AP modes transmit one linear polarization [e.g., horizontal (H)], and captures two backscattered intensities in H and vertical (V) polarizations (e.g., HH and HV). In addition to that, the DP modes preserve the differential phase between HH and HV. The CP mode [5] consists in transmitting one single polarization while preserving polarization diversity in reception. The CP mode transmits either a linear polarization oriented at $\pi/4$ or a circular polarization while receiving on two orthogonal polarizations. The FP information (i.e., the polarimetric coherency matrix) is further estimated iteratively by using assumptions of reflection-symmetry property of the observed scene and an extrapolation of the degree of coherence $\rho_{\rm HH\_VV}$ behavior.

The polarimetric indicators derived from the different polarimetric modes are listed in Table II. For the AP mode, six polarimetric indicators can be estimated from the two receiving channels leading to a six-component vector $V_{\rm AP}$. The DP and CP modes allow for the estimation of the covariance matrix $C = \langle (S_1 S_2)^{\rm T} (S_1 S_2)^* \rangle = \begin{bmatrix} C_{11} & C_{12} \\ C_{12}^* & C_{22} \end{bmatrix}$, where $\langle \ \rangle$ stands for the average over a local neighborhood and S_1 and S_2 are linear functions of the scattering matrix elements $S_{\rm HH}$, $S_{\rm HV}$ ($= S_{\rm VH}$ under scattering reciprocity assumption), and $S_{\rm VV}$. This matrix is defined from four real elements: two intensities (C_{11} and C_{22}) and the real and imaginary part of C_{12}. Table II gives details of the 13 polarimetric indicators estimated from these measurements, leading to the definition of the 13 components, $V_{\rm CP\_est}$ and $V_{\rm DP}$ for the CP and DP modes, respectively. The parameters H_2, α_2, and A_2, can be derived from C, analogous to H, A, and α for FP [14]. In the case where a $\pi/4$-oriented linear polarization is transmitted ($S_1 = S_{\rm HH} + S_{\rm HV}, S_2 = S_{\rm HV} + S_{\rm VV}$) or DP modes involving HH/HV ($S_1 = S_{\rm HH}, S_2 = S_{\rm HV}$) or VV/HV ($S_1 = S_{\rm HV}, S_2 = S_{\rm VV}$), the anisotropy A_2 corresponds to the degree of polarization of the backscattered wave. Finally, numerous indicators can be estimated from the reconstructed C matrix. A greedy analysis similar to those made in [8] allows for the definition of an optimal list of 21 indicators defining the vector $V_{\rm CP\_rec}$, which led to the best classification accuracy at both L- and
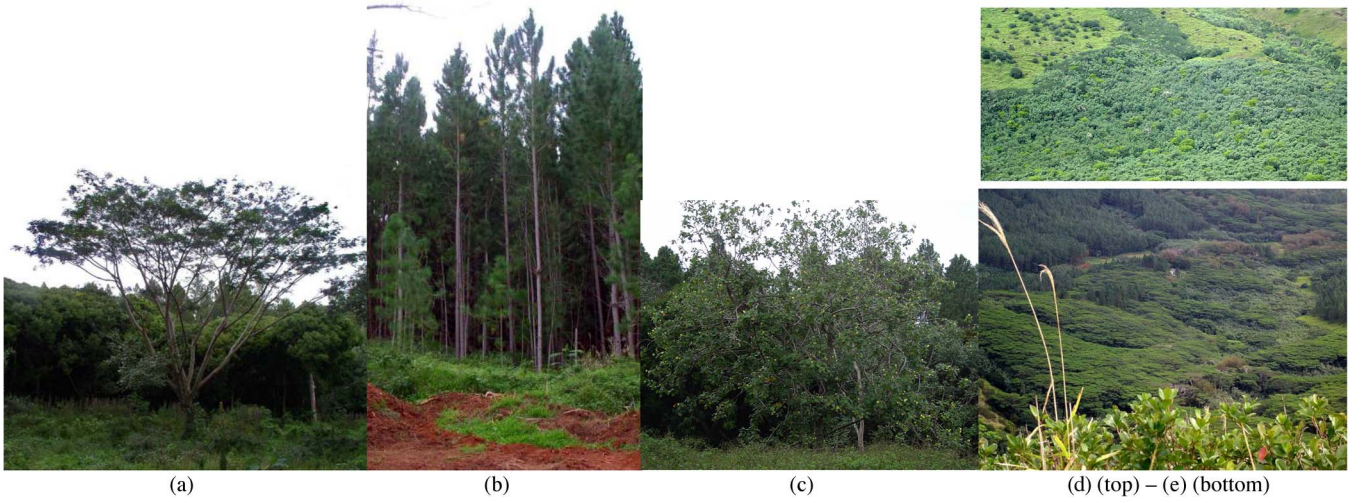
Fig. 1.   (a) Falcata, (b) Pinus, and (c) Purau individual trees. Global view showing (d) Purau and (e—middle left) Falcata and (e—up) Pinus patches.
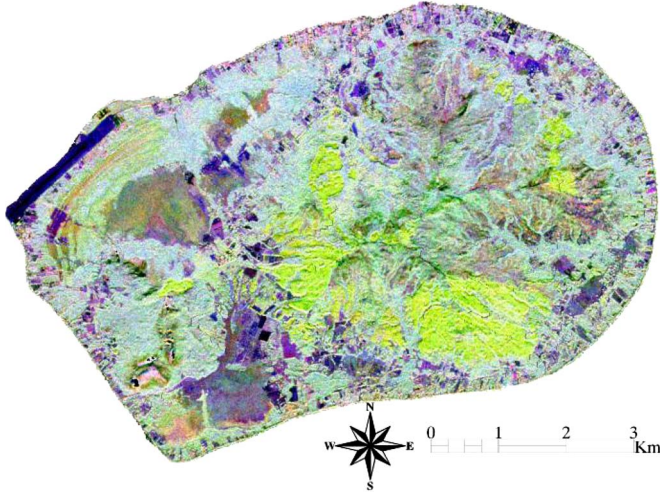

Fig. 2.   AIRSAR image of the Tubuai Island: The RGB channels correspond to L-HH, P-HV, and C-VV intensity channels, respectively.

TABLE II
POLARIMETRIC INDICATORS DERIVED FROM
THE DIFFERENT POLARIMETRIC MODES

Alternate Mode V_{AP}	Dual Mode V_{DP}; V_{CP_est}	Compact Mode V_{CP_rec}
		Estimated
I_{pq}, I_{rs}	C_{ij}	C_{ij}
I_{pq} / I_{rs}	C_{11} / C_{22}	c_{v_11}, c_{v_22}
S	S	$|\rho_{11\_22}|$
$c_{v\text{-}pq}$, $c_{v\text{-}rs}$	c_{v_11}, c_{v_22}	*Reconstructed*
	ρ_{11_22}	I_{HH}, I_{HV}, I_{VV}, I_{LL}, I_{LR}
	H_2, A_2, α_2	I_{HV}/I_{HH}, I_{LL}/I_{LR}
		c_{v_HH}, c_{v_VV}, c_{v_HV}, c_{v_LL}, c_{v_LR}
		$|\rho_{LL\_RR}|$
		m

P-band. It is composed of seven indicators directly estimated from the 2×2 C matrix and 14 additional indicators estimated from the 3×3 reconstructed coherency matrix. Among the latter, we find the different intensities in linear and circular polarization, their coefficient of variation, the modulus of the circular degree of coherence $|\rho_{LL\_RR}|$, with the subscript L

and R standing for left and right polarization, respectively, and the Euler parameter, m.

IV. RESULTS AND DISCUSSION

The iterative algorithm allowing for the reconstruction of the FP coherency matrix T_3 from the CP mode requires a local averaging of the polarimetric information. This averaging has been conducted over a 5×5 window. In order to allow a fair comparison between the different polarimetric modes, all of them were averaged using the same window, and the various polarimetric indicators were subsequently estimated.

Due to faster computational times and similar or higher performances by comparison with the others, the radial basis function kernel has been retained for the SVM algorithm with the same parameter values as in [8], i.e., with $\sigma = 0.5$ defining the Gaussian kernel width and a cost parameter $C = 1000$. Each classification is made with the same training and validation data sets. The number of training and control samples is given by Table I. In order to better account for the differences of population sizes, as in this case, the classification accuracy is given by the mean producer accuracy (MPA). It represents the mean of the producer accuracy (PA) of the seven classes, each expressed in percent. The PA is, for a given class, the ratio between the number of pixels well classified and the total pixel number of the class.

The classification accuracy obtained with the different polarimetric modes for different frequency combinations is given by Table III. The maximum MPA value observed (99%) is not realistic since several approximations were made, such as reducing the diversity of the Tubuai landscape to only seven homogeneous classes. It has to be considered more like a reference value from which the other configuration are assessed.

A. Evaluation of Partial Polarimetric Modes

1) General Trends: As expected, FP gives the best results for all frequencies (MPA = 90% for L- and P-band), and the AP mode gives the poorest (MPA < 68%). The DP mode shows significant improvement with respect to the AP mode (10% and 5% higher for L- and P-band), highlighting the added value

TABLE III
CLASSIFICATION ACCURACY (MPA %) ASSOCIATED WITH
THE DIFFERENT PARTIAL POLARIMETRIC MODES

Band	Full Polarimetry V_{FP}	Compact Mode $V_{CP\,rec}$	Dual-Pol Mode V_{DP}			Alternate Pol. Mode V_{AP}		
			HH/ HV	VV/ HV	HH/ VV	HH/ HV	VV/ HV	HH/ VV
L	90	80	72	69	74	64	62	62
P	90	79	71	73	72	64	68	58
L+C	98	95	93	89	92	88	86	86
P+C	97	94	89	90	91	85	87	83
L+P	98	94	89	88	90	80	82	80
L+P+C	99	99	96	96	97	94	95	94

of the differential phase. The CP mode confirms its potential, as it gives the best results between the partial polarimetric modes (with MPA ranging between 79% and 99%). It appears (not shown here) that, on the whole, the AP mode allows for the discrimination between forest and nonforest; the DP mode allows, in addition, for the discrimination between low vegetation and bare soils, while the CP or FP modes allow for a better discrimination within the different forest species. It is worth noting that, for the AP or DP modes, similar performances are obtained regardless of the polarization configuration (HH/VV, HH/HV, or VV/HV). This may come from the particular nature of the studied forest types, which are apparently not characterized by double-bounce scattering effects, favoring the HH–VV configuration. MPA differences between polarization configurations are indeed generally less than 3% except for four cases: AP mode at P-band and when P- and C-band are combined, as well as DP mode at L-band and when L- and C-band are combined, where differences reach 10%, 4%, 5%, and 4%, respectively. More details about these differences are discussed later in this section.

2) CP Mode—Reconstruction Contribution: It is observed that, contrary to [15], V_{CP_rec} gives better performance than V_{CP_est}, with MPA values that are 8% higher. V_{CP_est} shows similar performance to V_{DP}, with MPA values that are 2% higher for the latter. Additional tests (not shown here) confirm that the same results are observed when only the 2×2 C matrix elements versus the five real elements (T_{11}, T_{22}, T_{33}, and the real and imaginary parts of T_{13}) of the T_3 matrix, after reconstruction, are considered. In that case, MPA differences are less than 2% at L- or P-band. This result, obtained either for the SVM algorithm or for the maximum likelihood classifier based on the Wishart distribution, is in concordance with [15]. The reconstruction improves the classification performance when additional polarimetric indicators are involved. This illustrates one of the assets of the SVM algorithm, which is to account for heterogeneous indicators without any *a priori* assumptions about their distribution. It has to be pointed out that the reconstruction algorithm allows for a much better improvement over other tropical sites that we analyzed mainly with PALSAR FP data. This is mainly because, for the lower PALSAR spatial resolution, reflection symmetry of the backscattering signal

(hypothesis on the basis of the reconstruction algorithm) is verified over the different vegetation types, which is not the case here [8].

3) Sensitivity to Different Polarizations for the Same Partial Polarimetric Mode: When comparing HH/VV (MPA = 58%) and VV/HV (MPA = 68%) configurations for AP mode at P-band, it is the guava specie that cannot be discriminated with the former (PA = 8%), while VV/HV allows a much better discrimination (PA = 47%). This difference is reduced when the L- or C-band are combined with the P-band. Significant improvement is observed at P-band with the addition of the differential phase, with a difference of MPA values of only 1% between VV/HV (73%) and HH/VV (72%) acquisitions in DP mode. Finally, it is the poor discrimination of Falcata (PA = 40%) that explains the MPA value of 69% for L-band VV/HV DP mode, i.e., 5% lower than the 74% observed for the HH/VV configuration.

B. Multiacquisition Contribution

This section assesses the combination of different polarization or frequency bands. The use of several frequency bands is of obvious interest when compared with single frequency data takes (Table III). The multifrequency-classification improvement is of particular interest for partial polarimetric acquisitions with an increase of MPA values of 31%, 23%, 19%, and 9% for AP, DP, CP, and FP modes, respectively. It is worth noting that the merging of two acquisitions available with ALOS and ASAR sensors, i.e., L-band in DP mode and C-band in VV polarization, leads to performance similar to L- or P-band FP, with MPA values equal to 93% and 90%, respectively. This can be considered for thematic studies which have to trade off between the width of coverage (i.e., in favor of multiple partial polarimetry acquisitions) and the informative content of the acquisition (in favor of FP)

Fig. 3 shows the multifrequency-classification results obtained by combining three intensity channels (and the associated coefficient of variation c_v) among the seven available linear polarization channels: HH, VV, and HV at L- and P-bands, with the addition of VV at C-band. MPA values range between 68% and 88%. The best performance is obtained with the combination of L_{HH}, P_{HV}, and C_{VV}. This is 2% lower than the 90% observed with either L-band or P-band FP. In addition to the intensity information, it is found that the addition of the coefficient of variation c_v (capturing textural information) improves the classification accuracy from 4% to 8%. Another major result is the significant contribution of the C-VV signal in addition to L- and P-band data. By using it, MPA values ranging between 81% and 88% are obtained, instead of values below 78% when only L- and P-band data are considered. It shows the utility of a short wavelength for dense forest discrimination (which was not really expected). More specifically, the C-band channel allows for a significant improvement of the discrimination between Pinus and Falcata species. It is also worth noting that two AP acquisitions at L- or P-band, which allow the acquisition in HH, HV, and VV polarization (MPA = 72% and 75%, respectively) lead to about the same performance as with one single frequency DP acquisition (MPA = 74% and 73% at

Fig. 3. Classification results when the three intensity channels (and the associated c_v) are combined among the seven linear polarized intensity channels (three for L- and P-bands and one corresponding to VV polarization at C-band).

L- and P-band, respectively), illustrating again the importance of the information carried by the differential phase.

V. CONCLUSION

This letter has assessed the different partial polarimetric radar modes acquired at various frequency bands for the SVM classification of natural vegetation in a tropical environment (Tubuai Island, French Polynesia). It is shown that the L- and P-bands give similar performance. The FP modes give the best results, and, when partial polarimetric modes are considered, the CP mode represents the optimal configuration, and the AP mode represents the worst. It is observed that two AP modes that together yield three different linearly polarized channels give similar results as one DP acquisition, illustrating the value of the polarimetric differential phase. It is further observed that the polarimetric configuration has limited impact on the classification performance, both for AP mode and DP mode images of the studied tropical vegetation.

The complementarity between different frequency bands is very strong, as shown by the combination of P-, L-, and C-bands. In that context, the launch of a P-band spaceborne FP SAR sensor, such as the European Space Agency P-band BIOMASS mission, enhancing the existing X-, C-, and L-band spaceborne missions, would be of prime interest. Finally, it appears that, despite a reduced penetration depth in the canopy, C-band brings major contribution for the classification.

REFERENCES

[1] A. Freeman and S. L. Durden, "A three component scattering model for polarimetric SAR data," *IEEE Trans. Geosci. Remote Sens.*, vol. 36, no. 3, pp. 963–973, May 1998.

[2] J. S. Lee, M. R. Grunes, and R. Kwok, "Classification of multi-look polarimetric SAR imagery based on complex Wishart distribution," *Int. J. Remote Sens.*, vol. 15, no. 11, pp. 2299–2311, Jul. 1994.

[3] S. R. Cloude and E. Pottier, "An entropy based classification scheme for land applications of polarimetric SAR," *IEEE Trans. Geosci. Remote Sens.*, vol. 35, no. 1, pp. 68–78, Jan. 1997.

[4] J. S. Lee, R. G. Mitchell, and E. Pottier, "Quantitative comparison of classification capability: Fully polarimetric versus dual and single-polarization SAR," *IEEE Trans. Geosci. Remote Sens.*, vol. 39, no. 11, pp. 2343–2351, Nov. 2001.

[5] J.-C. Souyris, P. Imbo, R. Fjortoft, S. Mingot, and J.-S. Lee, "Compact polarimetry based on symmetry properties of geophysical media: The $\pi/4$ mode," *IEEE Trans. Geosci. Remote Sens.*, vol. 43, no. 3, pp. 634–646, Mar. 2005.

[6] R. Touzi, "Compact versus fully polarimetric SAR," in *Proc. POLinSAR*, Frascati, Italy, Jan. 2009.

[7] S. Cloude, I. Woodhouse, K. Viergever, and J. Suarez, "Mapping Scotland with PALSAR: An assessment of the importance of L-band polarimetry," in *Proc. 2nd PI ALOS Symp.*, Rhodes, Greece, Nov. 2008.

[8] C. Lardeux, P.-L. Frison, C. Tison, J.-C. Souyris, B. Stoll, B. Fruneau, and J.-P. Rudant, "Support vector machine for multi-frequency SAR polarimetric data classification," *IEEE Trans. Geosci. Remote Sens.*, vol. 47, no. 12, pp. 4143–4152, Dec. 2009.

[9] C. J. Burges, "A tutorial on Support Vector Machines for pattern recognition," in *Data Mining Knowledge Discovery*, U. Fayyad, Ed. Norwell, MA: Kluwer, 1998.

[10] R. K. Raney, "Hybrid-polarity SAR architecture," *IEEE Trans. Geosci. Remote Sens.*, vol. 45, no. 11, pp. 3397–3404, Nov. 2007.

[11] C.-W. Hsu and C.-J. Lin, "A comparison of methods for multiclass support vector machines," *IEEE Trans. Neural Netw.*, vol. 15, no. 2, pp. 415–425, Mar. 2002.

[12] S. R. Cloude and E. Pottier, "A review of target decomposition theorems in radar polarimetry," *IEEE Trans. Geosci. Remote Sens.*, vol. 34, no. 2, pp. 497–518, Mar. 1996.

[13] J. R. Huynen, "Phenomenological theory of radar targets," Doctoral thesis, Delft Univ., Delft, The Netherlands, 1970.

[14] P. Imbo and J.-C. Souyris, "Assessment of partial polarimetry versus full polarimetry architectures for target analysis," in *Proc. EUSAR*, Munich, Germany, May 23–25, 2000.

[15] T. L. Ainsworth, J. P. Kelly, and J.-S. Lee, "Classification comparisons between dual-pol, compact polarimetric and quad-pol SAR imagery," *ISPRS J. Photogram. Remote Sens.*, vol. 64, no. 5, pp. 464–471, Sep. 2009.